Dear Author,

Here are the proofs of your article.

- You can submit your corrections **online**, via **e-mail** or by **fax**.
- For **online** submission please insert your corrections in the online correction form. Always indicate the line number to which the correction refers.
- You can also insert your corrections in the proof PDF and **email** the annotated PDF.
- For fax submission, please ensure that your corrections are clearly legible. Use a fine black pen and write the correction in the margin, not too close to the edge of the page.
- Remember to note the **journal title**, **article number**, and **your name** when sending your response via e-mail or fax.
- **Check** the metadata sheet to make sure that the header information, especially author names and the corresponding affiliations are correctly shown.
- **Check** the questions that may have arisen during copy editing and insert your answers/ corrections.
- **Check** that the text is complete and that all figures, tables and their legends are included. Also check the accuracy of special characters, equations, and electronic supplementary material if applicable. If necessary refer to the *Edited manuscript*.
- The publication of inaccurate data such as dosages and units can have serious consequences. Please take particular care that all such details are correct.
- Please **do not** make changes that involve only matters of style. We have generally introduced forms that follow the journal's style.
  Substantial changes in content, e.g., new results, corrected values, title and authorship are not allowed without the approval of the responsible editor. In such a case, please contact the Editorial Office and return his/her consent together with the proof.
- If we do not receive your corrections **within 48 hours**, we will send you a reminder.
- Your article will be published **Online First** approximately one week after receipt of your corrected proofs. This is the **official first publication** citable with the DOI. **Further changes are, therefore, not possible.**
- The **printed version** will follow in a forthcoming issue.

Please note

After online publication, subscribers (personal/institutional) to this journal will have access to the complete article via the DOI using the URL: http://dx.doi.org/[DOI].
If you would like to know when your article has been published online, take advantage of our free alert service. For registration and further information go to: http://www.springerlink.com.

Due to the electronic nature of the procedure, the manuscript and the original figures will only be returned to you on special request. When you return your corrections, please inform us if you would like to have these documents returned.

Metadata of the article that will be visualized in OnlineFirst

ArticleTitle	On the Use of Computational Fluid Dynamics to Investigate Aerosol Dispersion in an Industrial Environment: A Case Study	
Article Sub-Title		
Article CopyRight	Springer Science+Business Media B.V. (This will be the copyright line in the final PDF)	
Journal Name	Boundary-Layer Meteorology	

Corresponding Author	Family Name	**Fossum**
	Particle	
	Given Name	**H. E.**
	Suffix	
	Division	
	Organization	Norwegian Defence Research Establishment (FFI)
	Address	Kjeller, 2027, Norway
	Email	hannibal.fossum@ffi.no
Author	Family Name	**Reif**
	Particle	
	Given Name	**B. A. Pettersson**
	Suffix	
	Division	
	Organization	Norwegian Defence Research Establishment (FFI)
	Address	Kjeller, 2027, Norway
	Email	bjorn.reif@ffi.no
Author	Family Name	**Tutkun**
	Particle	
	Given Name	**M.**
	Suffix	
	Division	
	Organization	Norwegian Defence Research Establishment (FFI)
	Address	Kjeller, 2027, Norway
	Email	murat.tutkun@ffi.no
Author	Family Name	**Gjesdal**
	Particle	
	Given Name	**T.**
	Suffix	
	Division	
	Organization	Norwegian Defence Research Establishment (FFI)
	Address	Kjeller, 2027, Norway
	Email	thor.gjesdal@ffi.no

	Received	28 October 2010
Schedule	Revised	
	Accepted	21 February 2012

Abstract	Aerosol dispersion in the area surrounding an existing biological treatment facility is investigated using large-eddy simulation, with the objective to investigate the applicability of computational fluid dynamics to complex real-life problems. The aerosol sources consist of two large aeration ponds that slowly diffuse aerosols into the atmosphere. These sources are modelled as dilute concentrations of a non-buoyant non-reacting pollutant diffusing from two horizontal surfaces. The time frame of the aerosol release is restricted to the order of minutes, justifying a statistically steady inlet boundary condition. The numerical results are compared to wind-tunnel experiments for validation. The wind-tunnel flow characteristics resemble neutral atmospheric conditions with a Reynolds number, based on the boundary-layer thickness, of $Re_{\delta} \approx 2 \times 10^5$. The numerical inflow conditions are based upon the wind-tunnel flow field. The predicted decay of both the mean and root-mean-square concentrations are in good agreement with experimental data; at 3 m from the ground, the plume mean concentration 200 m downwind of the source is approximately 2% of the source strength. The numerical data in the near-surface layer (0–50 m from the ground) correspond particularly well with the wind-tunnel data. Tentative deposition simulations suggest that there seems to be little difference in the deposition rates of large (1.8×10^{-5} m) and small (3×10^{-6} m) particles in the near-field under the flow conditions considered.
Keywords (separated by '-')	Aerosols - Dispersion - Large-eddy simulation - Turbulence - Validation
Footnote Information	

Boundary-Layer Meteorol
DOI 10.1007/s10546-012-9711-z

ARTICLE

On the Use of Computational Fluid Dynamics to Investigate Aerosol Dispersion in an Industrial Environment: A Case Study

H. E. Fossum · B. A. Pettersson Reif · M. Tutkun · T. Gjesdal

Received: 28 October 2010 / Accepted: 21 February 2012

Abstract Aerosol dispersion in the area surrounding an existing biological treatment facility is investigated using large-eddy simulation, with the objective to investigate the applicability of computational fluid dynamics to complex real-life problems. The aerosol sources consist of two large aeration ponds that slowly diffuse aerosols into the atmosphere. These sources are modelled as dilute concentrations of a non-buoyant non-reacting pollutant diffusing from two horizontal surfaces. The time frame of the aerosol release is restricted to the order of minutes, justifying a statistically steady inlet boundary condition. The numerical results are compared to wind-tunnel experiments for validation. The wind-tunnel flow characteristics resemble neutral atmospheric conditions with a Reynolds number, based on the boundary-layer thickness, of $Re_\delta \approx 2 \times 10^5$. The numerical inflow conditions are based upon the wind-tunnel flow field. The predicted decay of both the mean and root-mean-square concentrations are in good agreement with experimental data; at 3 m from the ground, the plume mean concentration 200 m downwind of the source is approximately 2% of the source strength. The numerical data in the near-surface layer (0–50 m from the ground) correspond particularly well with the wind-tunnel data. Tentative deposition simulations suggest that there seems to be little difference in the deposition rates of large (1.8×10^{-5} m) and small (3×10^{-6} m) particles in the near-field under the flow conditions considered.

Keywords Aerosols · Dispersion · Large-eddy simulation · Turbulence · Validation

H. E. Fossum (✉) · B. A. P. Reif · M. Tutkun · T. Gjesdal
Norwegian Defence Research Establishment (FFI), 2027 Kjeller, Norway
e-mail: hannibal.fossum@ffi.no

B. A. P. Reif
e-mail: bjorn.reif@ffi.no

M. Tutkun
e-mail: murat.tutkun@ffi.no

T. Gjesdal
e-mail: thor.gjesdal@ffi.no

1 Introduction

Borregaard Ind. Ltd., located in Sarpsborg, Norway, is the world's leading supplier of wood-based chemicals, and waste water from their wood refinement plant is biologically treated according to environmental requirements legislated by the Norwegian Environmental Protection Agency. Here we consider the continuous release of aerosols from such a biological treatment facility.

The facility consists of two large open-air aeration ponds each containing about 30,000 m^3 of liquid, each having a diameter of approximately 40 m. In order to promote optimal growth of microorganisms achieving efficient degradation of various organic substances, the pond temperature is maintained constant at about 37°C. In addition, about 8.3 $m^3\,s^{-1}$ of constant temperature air (≈20°C) is circulated through each pond, giving rise to massive aerosol generation at the liquid surface. These aerosols, which potentially may contain microorganisms from the ponds, are emitted with low vertical velocity into the surroundings, and then transported and dispersed downwind by the wind field.

Liquid samples taken directly from these aeration ponds (Blatny et al. 2008, 2011), and samples of aerosols collected immediately above the liquid surfaces (Olsen et al. 2010), have all revealed the presence of the microorganism *Legionella* spp. Blatny et al. (2008) proved that Legionella-containing aerosols could be dispersed from the aeration ponds and transported at least 300 m downwind of the ponds. Epidemiological investigations in conjunction with outbreaks of Legionnaires disease among the population (Nguyen et al. 2006; Nygård et al. 2008) have even suggested that Legionella-containing aerosols may be transported up to 10 km from its source. The true source of Legionella-containing airborne aerosols that caused the largest outbreak of Legionnaires disease in Norway by inhalation has, however, not yet been unambiguously identified. During an outbreak in May, 2005, 10 people died and 56 patient cases were documented (Nygård et al. 2008).

The present study constitutes an integral part of a broader initiative to gain further insight into the dispersion and transport processes, and the microbiological characteristics, of aerosols emitted from the aeration ponds at Borregaard Ind. Ltd., Norway (cf. Blatny et al. 2008, 2011; Olsen et al. 2010). The aeration ponds considered in this study have been identified as two of several possible sources responsible for the outbreak in 2005.

The Legionella outbreaks occurred over several days. During the 2005 outbreak, the meteorological data generally showed wind conditions corresponding to a Reynolds number, based on the boundary-layer thickness δ, of $Re_\delta \sim 10^8$ and neutral to unstable conditions. The flow characteristics used herein were chosen such that the wind-tunnel experiments and computer simulations ensure that conditions are no more favourable to aerosol mixing than the actual meteorological conditions during the outbreak. This was achieved by considering isothermal conditions at a similar Re_δ.

There exists a plethora of modelling approaches to simulate aerosol dispersion. Simple computational models based on e.g. the Gaussian-puff approach (Sykes and Gabruk 1996) are frequently used to characterize contaminant dispersion in the atmospheric boundary layer. These should normally not be applied in microscale complex urban or industrial environments since the fine-scale geometrical features are of crucial importance.

Fuelled by the need for «fast» urban dispersion models, a number of approaches to extrapolate the use of the puff models to urban terrain have been proposed (e.g. Taylor and Salmon 1993; Kaplan and Dinar 1996). Although progress has been made in recent years, there are still very large uncertainties associated with the use of these techniques in complex built-up terrain. Despite its computational cost, computational fluid dynamics (CFD) is increasingly being used in urban dispersion applications. As pointed out by Lee et al. (2000), however,

Journal: 10546-BOUN Article No.: 9711 MS Code: BOUN901.3 TYPESET DISK LE CP Disp.:2012/2/25 Pages: 20 Layout: Small

the application of CFD in urban environments highlights a number of modelling issues that need to be addressed in order to warrant its use. Many CFD studies addressing dispersion in urban or industrial environments are based on the assumption that the flow field is statistically steady. The steady-state Reynolds-averaged Navier–Stokes (RANS) approach is thus frequently used, cf. e.g. Lien and Yee (2004), Coirier et al. (2005), Lien et al. (2006), Santiago et al. (2007).

Lien et al. (2006) concluded that the standard linear eddy-viscosity k–ε model was perhaps the simplest complete turbulence model that could be used for urban flow predictions. They also noted, however, that while the mean velocity field can be quite well predicted using this approach, the turbulence kinetic energy seems in general to be under-predicted. It thus follows that also the mixing process caused by irregular velocity fluctuations may be poorly represented. Ad hoc modifications of the RANS model can be devised to improve the predictions of the turbulence kinetic energy, cf. e.g. Wang et al. (2008), though the general applicability of these modifications to arbitrary complex building structures and variation in topography are questionable.

As already alluded to, the application of CFD for dispersion and transport modelling in complex urban or industrial environments are confronted with many challenges. The effects on the flow field of the interaction between the blockage caused by building structures and the atmospheric boundary layer (ABL) are crucially important and need to be accounted for in the computational model.

From a modelling perspective, the dominating effects are, (i) kinematic blocking of velocity components normal to solid surfaces, and (ii) non-local effects caused by pressure reflections (cf. e.g. Durbin and Reif 2002). The latter dominates in the ABL where it greatly modifies the turbulence anisotropy and consequently also the dispersion process. Kinematic blocking dominates the local flow conditions in densely built-up areas with tall buildings and produces street canyon (channeling) effects, flow separation, and the subsequent generation of unsteady wakes.

The mesoscale atmospheric events affecting the incoming ABL flow can, to a good approximation, be treated as statistically steady when considering releases of up to an hour. The dominating fluid dynamical processes within urban terrain are however essentially statistically unsteady.

There are three dominating sources of this flow unsteadiness: (i) instantaneous spatial and temporal variations of the energy containing large-scale motion of the incoming flow, (ii) the flow in the wake region downstream of buildings, and (iii) self-generated unsteadiness related to the emission itself. The ABL is characterized by a continuous range of spatial scales from a few tens of millimetres up to several hundreds of metres, with temporal scales varying from a fraction of a second up to a few tens of minutes. The large-scale time variation of building wakes can be up to an order of some minutes. These temporal effects are crucially important in cases where the source release time is in the order of, say, one hour or less, which is typically the case for accidental or intentional releases.

In an effort to overcome the challenges associated with unsteady mixing, which is believed to play a crucial role in order to accurately predict contaminant transport, the present study adopts the large-eddy simulation (LES) approach that, at least conceptually, resolves the temporal and spatial variation of the large energetic scales in the turbulent boundary layer. The objective is to increase our understanding of the near-field transport ($<$500 m) of aerosols emitted from aeration ponds in general, and for those at Borregaard Ind. Ltd. specifically, that potentially carry microbiological material that may result in disease. The present study thus addresses a real-life scenario characterized by a considerable separation of spatial and temporal scales. The computational effort uses what is practically achievable with the available

Journal: 10546-BOUN Article No.: 9711 MS Code: BOUN901.3 TYPESET DISK LE CP Disp.:2012/2/25 Pages: 20 Layout: Small

computer resources. The simulation results are verified by data from recent wind-tunnel tests carried out at the Environmental Flow Research Laboratory (EnFlo) at the University of Surrey, Guildford, UK.

The primary objectives are (i) to verify whether CFD is a suitable tool for investigating near-field aerosol transport in the ABL, and if so (ii) to use CFD results to shed light on the role of aeration ponds during the largest outbreak of Legionella ever recorded in Norway. The conclusions drawn will be determined by how well the computational model predicts various aspects of the flow and concentration fields. As such, comments regarding the physical phenomena of the flow will also be included in the analysis of the results, as well as in the conclusions. In the present study these phenomena are discussed in the context of model verification, not as an independent topic. However, if a computational model is to be of any use in later investigations into the physics of aerosol dispersion, it is imperative that realistic physical phenomena emerges from the model. Hence, part of this paper also focuses on the dispersion features themselves.

2 Problem Characterization

2.1 Geometry

The full-scale dimensions of the computational domain ($L_x \times L_y \times L_z$) are approximately $700 \times 800 \times 400\,\mathrm{m}^3$, where the global wind direction is in the y-direction and z is the vertical direction. The wind-tunnel model is of scale 1:300, i.e. approximately $2.3 \times 2.7 \times 1.3\,\mathrm{m}^3$, and these are also the actual dimensions used in the computer simulation model. Most buildings in the area belong to the industrial plant. The surrounding landscape consists of grasslands with a few trees, some sloping hills and a river, see Fig. 1. See also Sect. 2.3 for topographical details, and Sect. 3.1 for details of the computational mesh.

Aerosols are released from the two aeration ponds marked in red (dark) in Fig. 1. The full-scale height of the ponds is approximately 12 m, with diameter around 42 m. As thermal effects are ignored and the source is considered dilute, no buoyancy or two-way coupling effects are likely to be present. In real life, the ponds contain water (≈37°C), from which aerosols diffuse into the atmosphere with very small vertical velocity. It is assumed that the temperature difference between the pond and the surrounding air has an insignificant impact on the surrounding flow. The aerosols are considered small and their concentration sufficiently dilute that they do not influence the wind field.

2.2 The Atmospheric Boundary Layer

As previously stated, the current numerical simulation and wind-tunnel experiment are performed under neutral conditions, assuming constant temperature in the entire domain. Potential humidity effects are also neglected. These conditions ensure at least as much mixing as the real-life conditions observed during the outbreaks, in particular the largest in 2005. It should be recalled that the meteorological conditions during the outbreak were neutral to unstable. The main motivation for using such conditions in the wind tunnel is to derive a conservative estimate for the maximum mean concentration of Legionella downstream of the source. The incoming wind field is created in the wind tunnel so as to imitate a real-life atmospheric field (cf. e.g. Robins et al. 2001) with a Reynolds number $Re_\delta \approx 2 \times 10^5$. In

Journal: 10546-BOUN Article No.: 9711 MS Code: BOUN901.3 TYPESET DISK LE CP Disp.:2012/2/25 Pages: 20 Layout: Small

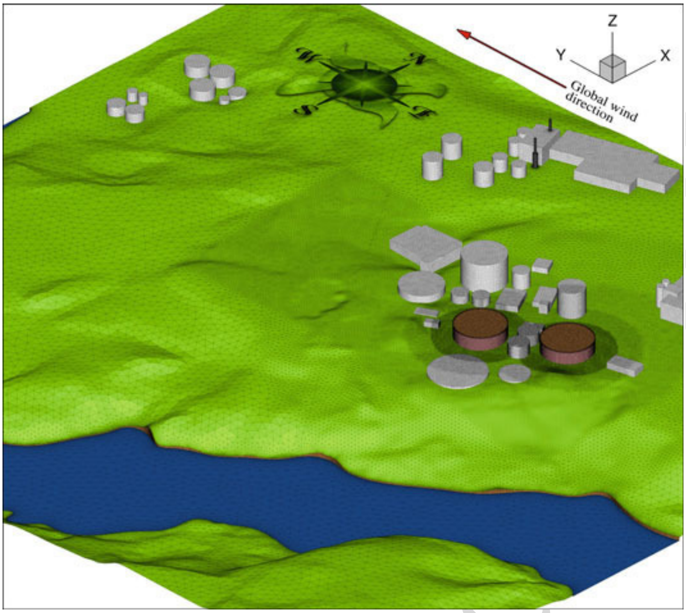

Fig. 1 The computational mesh of the Borregaard Ind. Ltd. geometry. Full-scale dimensions ($L_x \times L_y \times L_z$) are approximately $700 \times 800 \times 400\,\mathrm{m}^3$. Cell sizes range from 0.5 to 7.5 m. The aeration ponds are marked in *red*

the computer simulation, the incoming wind field is generated using wind-tunnel data (see Sect. 3.4.1).

Exact data for the atmospheric conditions during the Leigionella outbreak in 2005 are not available. However, during the entire period of the outbreaks (about a week), the wind field was in the high Reynolds number range ($Re_\delta \sim 10^8$), and the boundary layer was neutral or unstable. The Reynolds number in the wind tunnel is thus lower than that of the real-life atmospheric boundary layer, though the flow is still in the high Reynolds number range, in which scalar dispersion is relatively independent of the Reynolds number. As mentioned previously, in the context of the present study, an approach that ensures the same or greater mixing than the real case is more important than merely attempting to recreate or model real-life conditions exactly.

For validation purposes the same conditions as in the wind tunnel must be used in the computer simulation. Once successfully verified, the computational approach may be used to conduct further studies in which e.g. the atmospheric conditions are altered, or different aerosol sizes are considered. This is, however, outside the scope of the present study.

2.3 Topography

The present topography differs significantly both from entirely unpopulated areas and densely populated cities. However, some conclusions drawn from this study will potentially have implications for similar problems with domains of comparable sizes. Indeed, the verification of simulation methodology obtained herein will in large part be valid also for different topographies. Note that the results themselves, though, cannot be translated to different

Journal: 10546-BOUN Article No.: 9711 MS Code: BOUN901.3 TYPESET DISK LE CP Disp.:2012/2/25 Pages: 20 Layout: Small

Table 1 Key features of the topography, in full scale

Building count	45
Average building area	539.43 m^2
Average building height	10.80 m
Standard deviation of building height	6.57 m
Building density for bounding box of buildings	1.76×10^{-4} bld m^{-2}
Building density for entire domain	8.19×10^{-5} bld m^{-2}
Minimum landscape elevation	−3 m
Maximum landscape elevation	53 m
Average landscape elevation	21.9 m
Standard deviation of landscape elevation	17.6 m

topographies. A few basic features of the topography used in this study are nevertheless summarized in Table 1.

3 Computational Modelling

3.1 Mesh Generation

A mesh consisting of 4.2×10^7 cells has been used to discretize the geometry, cf. Fig. 1. The height of the domain is the same as in the wind tunnel, but the computational domain is smaller than the wind-tunnel dimensions in the horizontal directions. Adequate space between the region of interest and the domain boundaries is ensured, following the directions of the COST Action 732 guidelines (cf. e.g. Franke et al. 2011).

Comparisons with simulations on a coarser mesh[1] suggested that the flow patterns globally were reasonably unaffected by the grid. It should be noted that this case constitutes an approximation of a real-life scenario with significant scale separations. Grid independence is virtually impossible, but the assessment of the present grid suggests that is resolves the most dominant flow features. Reports of non-dimensional distance $y_+ = d_y u_* / \nu$ from the ground, where $u_* = (\tau_w / \rho)^{1/2}$ is the friction velocity given in terms of density ρ and wall stress τ_w, d_y is distance from the wall, and ν is kinematic viscosity, implied that the near-wall resolution was adequate ($y_+ < 50$) for a built environment.

The aerosol sources, i.e. the surfaces of the aeration ponds, each comprised more than 13,000 cell faces, with a surrounding grid resolution of approximately 0.5 m.

3.2 Turbulence Modelling

The LES model, utilizing the dynamic Smagorinsky approach, has been used, as implemented in the commercial software ANSYS Fluent 12.0 (Fluent 6.3 User's Guide 2006). For a Newtonian, incompressible flow, the filtered equations for conservation of momentum and mass can be written as

$$\frac{\partial U_i}{\partial t} + U_j \frac{\partial U_i}{\partial x_j} = -\frac{1}{\rho}\frac{\partial P}{\partial x_i} + \nu \frac{\partial^2 U_i}{\partial x_j \partial x_j} - \frac{\partial \tau_{ij}}{\partial x_j}, \tag{1}$$

$$\frac{\partial U_i}{\partial x_i} = 0, \tag{2}$$

[1] The overall cell density in the coarse mesh was only 14% of that in the fine mesh. However, near the ground, the coarse mesh had a cell density of about 70% of the fine mesh.

Journal: 10546-BOUN Article No.: 9711 MS Code: BOUN901.3 TYPESET DISK LE CP Disp.:2012/2/25 Pages: 20 Layout: Small

respectively, where $U_i(\mathbf{x}, t)$ and $P(\mathbf{x}, t)$ denote the filtered velocity component in the x_i direction and the filtered pressure field, respectively, and ν is the kinematic viscosity. $\tau_{ij} = \overline{u_i' u_j'} - U_i U_j$ is the residual stress, or subgrid-scale, tensor, which physically represents the impact of the unresolved velocity components on the computationally resolved velocity field. The present study utilizes the Smagorinsky model (cf. e.g. Kim 2004), given by

$$\tau_{ij} - \tfrac{1}{3}\tau_{kk}\delta_{ij} = -2\nu_t \overline{S}_{ij}, \tag{3}$$

where $\nu_t = L_s^2|S|$ is the subgrid-scale turbulent viscosity. The length scale is $L_s = \min(\kappa d_y, C_s V^{1/3})$, where κ is the von Kármán constant, d_y is the distance to the closest wall, and V is the volume of the computational cell. The Smagorinsky constant C_s is determined dynamically and is computed based on the resolved scales of motion. The rate-of-strain tensor for the resolved scale is given by $\overline{S}_{ij} = \frac{1}{2}(\frac{\partial U_i}{\partial x_j} + \frac{\partial U_j}{\partial x_i})$.

3.3 Dispersion Modelling

Two different dispersion modelling strategies have been adopted. Firstly, a scalar-transport model has been employed to simulate the plume evolutions. Secondly, a Lagrangian discrete-particle approach has been used to investigate particle ground deposition. Experimental data are used to validate the plume evolution up to distances of 500 m downwind of the aeration ponds (see Sect. 4), and representative aerosol sizes experimentally obtained from full-scale measurements (Blatny et al. 2011) are used in the Lagrangian approach.

3.3.1 Scalar Transport

The transport of passive scalars, such as the tracer gas used in the wind tunnel, is governed by the advection-diffusion equation

$$\frac{\partial c}{\partial t} + U_i \frac{\partial c}{\partial x_i} = \nabla^2(\alpha_c c + \tfrac{\nu_T}{Sc_T} c), \tag{4}$$

where $c = c(\boldsymbol{x}, t)$ represent the scalar field and α_c denotes the scalar molecular diffusivity, and the last term represents a model for subgrid-scale turbulent diffusion. In the present study, the subgrid-scale turbulent Schmidt number Sc_T is obtained through the dynamic procedure described in Germano et al. (1991).

3.3.2 Particle Transport

The discrete-particle transport model incorporates inertia and gravity effects inherently ignored in the scalar transport model. The displacement of a given particle follows from integrating the force balance on that particle, which can be written in a Lagrangian reference frame. For example, in the tangential direction x_p of the particle trajectory, the force balance can be written as

$$\frac{\mathrm{d}u_p}{\mathrm{d}t} = F_D(u_{x_p} - u_p) + \frac{g_{x_p}(\rho_p - \rho)}{\rho_p} + F_{x_p}, \tag{5}$$

where u_{x_p} and u_p are the fluid and particle velocities, respectively, in the x_p direction. The former is obtained from the LES flow field. F_D denotes the drag force in the x_p direction

Journal: 10546-BOUN Article No.: 9711 MS Code: BOUN901.3 TYPESET DISK LE CP Disp.:2012/2/25 Pages: 20 Layout: Small

on the particle exerted by the wind field, ρ and ρ_p are the densities of the fluid and the particle, respectively, and g_{x_p} is the gravitational acceleration in the x_p direction. F_{x_p} involves pressure-gradient and virtual-mass effects, i.e.

$$F_{x_\mathrm{p}} = \frac{1}{2}\frac{\rho}{\rho_\mathrm{p}}\frac{\mathrm{d}}{\mathrm{d}t}(u_{x_\mathrm{p}} - u_\mathrm{p}) + \left(\frac{\rho}{\rho_\mathrm{p}}\right) u_{\mathrm{p},i}\frac{\partial u_{x_\mathrm{p}}}{\partial x_{\mathrm{p},i}}. \tag{6}$$

The drag force is modelled using a spherical drag law, i.e.

$$F_\mathrm{D} = \frac{18\mu}{\rho_\mathrm{p} d_\mathrm{p}^2}\frac{C_\mathrm{D} Re}{24}, \tag{7}$$

where d_p is the diameter of the particle, and C_D is the drag coefficient, in the present study given by $C_\mathrm{D} = a_1 + a_2/Re + a_3/Re^2$. The constants a_1, a_2 and a_3 apply to smooth spherical particles over several spatial ranges given by Morsi and Alexander (1972). Also in the above, Re is the slip velocity Reynolds number, defined as $Re \equiv \rho d_\mathrm{p}|u_\mathrm{p} - u_{x_\mathrm{p}}|/\mu$.

In its original form, integration of Eq. 5 only yields the particle velocity based on the resolved scales of motion. To account for the subgrid scales, a stochastic model is applied, through which a fluctuating velocity component is added to the fluid velocity used in Eq. 5 at every timestep. The fluctuating velocity components are discrete piecewise constant functions of time, where their random value is kept constant over an interval of time given by the characteristic lifetime of the eddies, computed from the resolved field.

In this study, thermophoretic forces, Brownian forces, and lift forces are assumed to be insignificant and are therefore neglected. Also, effects such as evaporation, agglomeration, and particle collisions are neglected. The particle release in this study can be considered dilute, making these simplifying assumptions approximately valid (Elgobashi 1994).

3.4 Numerical Approach

The pressure-based solver in Fluent is used. The second-order accurate bounded central-differencing scheme has been used for the momentum equations, while the pressure-velocity coupling is handled by the semi-implicit method for pressure-linked equations (commonly known as the SIMPLE scheme). A second-order implicit Euler temporal scheme is used. The Lagrangian transport equations are integrated through a combination of a lower order implicit Euler scheme, which is unconditionally stable, and a higher-order semi-implicit trapezoidal scheme. An automated switch determines which scheme to use, depending on how far the particle is from hydrodynamic equilibrium.

The temporal resolution, Δt, was estimated using the large-scale turbulent time scale, i.e. $\tau = L/U = 0.0146$ s, where U is the mean inlet velocity at height L from the ground. The timestep was set to be $\Delta t = \tau$. The turbulent length scale L, also used to determine eddy sizes at the inlet, is estimated as 2/3 of pond height, i.e. approximately 7.3 m (full scale), cf. Fig. 1.

3.4.1 Boundary Conditions

All vertical boundaries of the domain, except building walls, are set as pressure outlets, which allows for an unsteady flow evolution, and they allow particles to escape. No-slip conditions are used on solid surfaces, such as the ground, and walls and roofs of the buildings. The top surface of the computational domain is defined as a symmetry plane, with an escape condition for discrete particles. The top boundary is sufficiently far from the ground, such that any influence of the symmetry assumption is negligible on the solution. The pond surfaces,

Journal: 10546-BOUN Article No.: 9711 MS Code: BOUN901.3 TYPESET DISK LE CP Disp.:2012/2/25 Pages: 20 Layout: Small

where the aerosol generation takes place, are set as no-slip walls, but with a concentration of 100% polluted air (with the same dynamical properties as air), and a reflection condition for discrete particles that are placed on the surfaces when running the discrete-particle model.

The inlet conditions required special consideration in order to be comparable to the experimental conditions. The measured wind profile at a point close to the inlet of the simulation domain was interpolated by a cubic function up to the maximum measuring height. Above this height, the free-stream velocity from the wind-tunnel inlet was used.

The turbulence properties at the inlet were estimated via measurements of velocity-fluctuation correlations in the streamwise and vertical directions, taken at the same position as the mean flow-field measurements. That is, $\overline{v'^2}$, $\overline{w'^2}$ and $\overline{v'w'}$ were set as the averages of measured experimental values, where v' is the streamwise component and w' is the vertical component. The remaining subgrid stress components were determined by assuming axisymmetric turbulence, i.e. $\overline{u'^2} = \overline{w'^2}$, $\overline{u'v'} = \overline{v'w'}$ and $\overline{u'w'} = 0$. It should be noted that due to lack of experimental data, the present velocity inlet conditions are only approximate. The presence of buildings, however, is believed to reduce the effect of the inlet profile, at least close to the ground.

Finally, from comparisons of streamwise velocity fluctuations v' to the mean free-stream streamwise velocity V at the measuring location used for the inlet condition, it was found that $|v'/V| \approx 0.1$, implying a turbulence intensity of about 10%. This, along with the aforementioned length scale L, was also specified as a parameter used to generate eddies at the inlet through a spectral synthesizer method.

3.4.2 Statistics

Prior to the statistical sampling, the flow evolved for 4,000 timesteps (i.e. for 1 min) from its initial conditions. Statistics were gathered for more than 14,000 timesteps, representing approximately 1,400 uncorrelated samples, or 3.5 min of simulation time. It is important to note that only the statistics of the flow and dispersion are considered in this study. There is virtually an infinite number of possible realizations of the flow pattern in real life, hence only a statistical prediction is meaningful. In that respect, care must be taken to collect statistics long enough to obtain converged statistical data, but rapid enough that boundary conditions do not change significantly. In the case of a controlled computer simulation and wind-tunnel experiment, as is the case in the present study, such conditions can be controlled and thus cause no problems.

For the discrete particle transport, preliminary tests showed that the same timestep could be used as for the flow simulations. During an initial phase of five timesteps (0.073 s), about 275,000 particles were placed at rest on the surfaces of the two aeration ponds. The total number of released particles in the simulation was equally divided between two dominating particle sizes obtained in recent field measurements (cf. Blatny et al. 2011): 18 and 2 μm. After the initial phase, all particles were tracked until most (>99%) had left the computational domain or were trapped.

It should be noted that each particle in the simulation does not necessarily correspond to one particle in full scale. In fact, a scaling with the measured particle count, preferably at several locations, is necessary to provide the real particle counts (e.g. in parts per million or some other measure). However, regardless of scaling, once the simulation method has been verified, the simulations provide valuable information about the pattern and speed of the propagation of particles.

Journal: 10546-BOUN Article No.: 9711 MS Code: BOUN901.3 TYPESET DISK LE CP Disp.:2012/2/25 Pages: 20 Layout: Small

In order to compare the computational results with wind-tunnel concentration measurements it was necessary to use the scalar field approach. The statistical convergence using particles is very slow and thus computationally demanding, and the scalar transport approach offers a viable alternative. These two approaches are in fact formally equivalent in the limit of statistical convergence if particle mass can be neglected (and particle collisions, agglomeration and break-ups ignored). The latter requirement is fulfilled here since $St \ll 1$. The scalar field approach can, however, not be used to quantify aerosol deposition. The discrete particle approach was therefore adopted.

It should finally be noted that also in the case of species transport, Δt was set equal to the flow simulation timestep, again verified by similar methods as in the flow calculations. Statistics were gathered for more than 14,000 time steps (about 3.5 min).

4 Wind-Tunnel Measurements

A 1:300 scale wind-tunnel model of the terrain and buildings surrounding Borregaard was manufactured using high density polyurethane foam. The model, which represents approximately 1 km^2 in full scale, was assembled in the large atmospheric wind tunnel at the Environmental Flow Research Centre at the University of Surrey, Guildford, UK (cf. e.g. Robins et al. 2001). The wind tunnel has a 20 m long test section with a cross-sectional area of $3.5 \times 1.5\,\mathrm{m}^2$, with the first 10 m used for flow conditioning purposes. The tunnel can be operated at a free-stream velocity between 0.8 and 2.5 $\mathrm{m\,s^{-1}}$. A large number of planar roughness elements was mounted on the wind-tunnel floor upstream of the model to create a realistic incoming boundary layer. The circular model (3.4 m in diameter) was mounted on a rotatable disk on the tunnel floor whereby different flow directions could be tested by rotating the model.

In this study we focus on one flow direction and one flow speed (corresponding to $Re_\delta = 2 \times 10^5$). The wind-tunnel model incorporates many details of the terrain, including the river Glomma, and the major building structures at Borregaard, but for practical purposes the model had to be simplified. For instance forested areas and other vegetation present on site or in its immediate vicinity were removed, as well as small buildings. The wind-tunnel measurements presented here are limited to isothermal atmospheric conditions.

The released contaminant consisted of a mixture of air with a trace of propane (C_3H_8). In order to simulate the aerosol generation at the surface of the ponds, each pond was filled with a large number of small spherical high-density polyethylene balls (3 mm in diameter) in order to create a porous media through which the tracer gas could slowly diffuse into the surroundings. The tracer could thus be released from the aeration ponds uniformly over the cross-sectional area of each pond and with a very small vertical velocity.

The choice of using a tracer gas in place of particles is justified in this case since the particle inertia can be neglected. The Stokes number St, defined as the ratio between the particle relaxation time ($\tau = \rho_\mathrm{p} d_\mathrm{p}^2/(18\mu)$) and the characteristic time scale (t) for the wind field, is $\ll 1$. The particle relaxation time scale is computed using the aerosol (H_2O) density ($\rho_\mathrm{p} = 998\,\mathrm{kg\,m^{-3}}$ at 20°C), the molecular viscosity of the surrounding air ($\mu_\mathrm{air} = 1.67 \times 10^{-5}\,\mathrm{N\,s\,m^{-2}}$ at 20°C), and the particle diameter (d_p): $\tau \approx 9.3 \times 10^6 d_\mathrm{p}^2$. The characteristic time scale for the wind field can be estimated to be of the order of $t \approx 10^{-1}$ s, which, in combination with an aerosol diameter $d_\mathrm{p} < 2 \times 10^{-5}$ m, gives $St \approx 3.7 \times 10^{-2} \ll 1$.

Laser Doppler anemometry (LDA) was used to measure the fluctuating velocity field whereas the concentration measurements were conducted using a fast flame ionisation

Journal: 10546-BOUN Article No.: 9711 MS Code: BOUN901.3 TYPESET DISK LE CP Disp.:2012/2/25 Pages: 20 Layout: Small

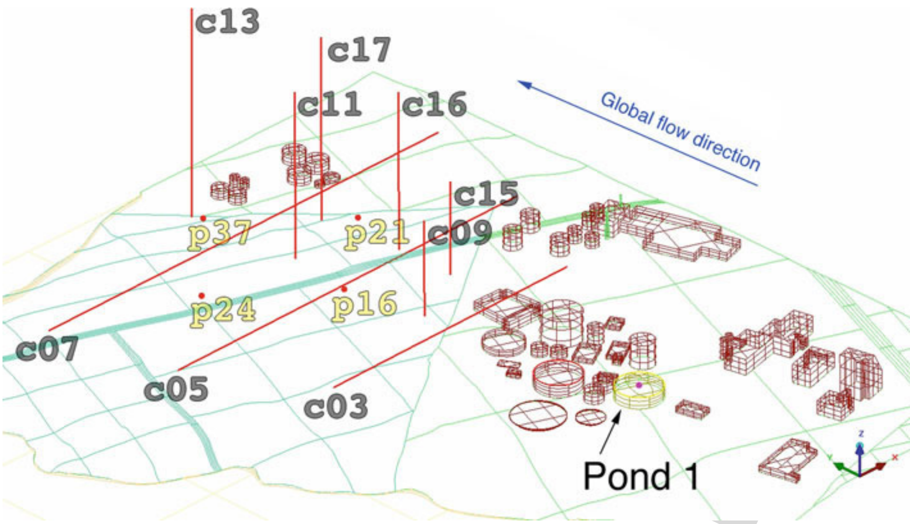

Fig. 2 An overview of the measuring locations. The *points* labeled `pNN` represent vertical measuring lines for the velocity, and the *lines* labeled `cNN` represent measuring lines for the concentration field. The global wind direction is along the y-axis

detector (FFID) at a sampling frequency of 200 Hz. Ground level concentrations, 0.010 m above the model surface (corresponding to approximately 3 m above the ground in full scale), were measured, as well as vertical variations of the concentration. The data were collected in blocks, in total 200 at each measurement position, in order to ensure statistical convergence of the data.

5 Results and Discussion

Considering the complexity and dimensions of the geometry, the results generally agreed well with experimental data, as will be seen shortly. The greatest discrepancies, seen in the turbulent fluctuations of the flow, are most likely due to somewhat inaccurate boundary conditions. The measuring locations used in this study are indicated in Fig. 2. All distances in all directions in the following figures are measured from the centre of the surface of pond 1 in Fig. 2.

The flow field results are scaled with the inlet free-stream velocity, whereas the contaminant field results are scaled with the mean concentration source strength. However, the source characteristics of the simulations and the experiments differ (cf. Sects. 4 and 3.4.1). Therefore, an additional scaling is used, in order to scale the experimental concentration field to the simulation field. This scaling factor is applied globally and is based on the average ratio of experiment to simulation plume maximum values for six spanwise lines (`c03`, `c05` and `c07` and three other similar lines spread uniformly downstream the source). The scaling factor is set as 2.8057×10^{-4}.

5.1 Flow Field

Figure 3a and c shows mean streamwise velocities along the vertical lines situated at `p03` and `p16`, and `p21` and `p24`, respectively. Note that in the former figure, the two locations lie along a streamwise line, and in the latter figure, the locations lie along a spanwise line

Journal: **10546-BOUN** Article No.: **9711** MS Code: **BOUN901.3** ☐ TYPESET ☐ DISK ☐ LE ☐ CP Disp.:**2012/2/25** Pages: **20** Layout: **Small**

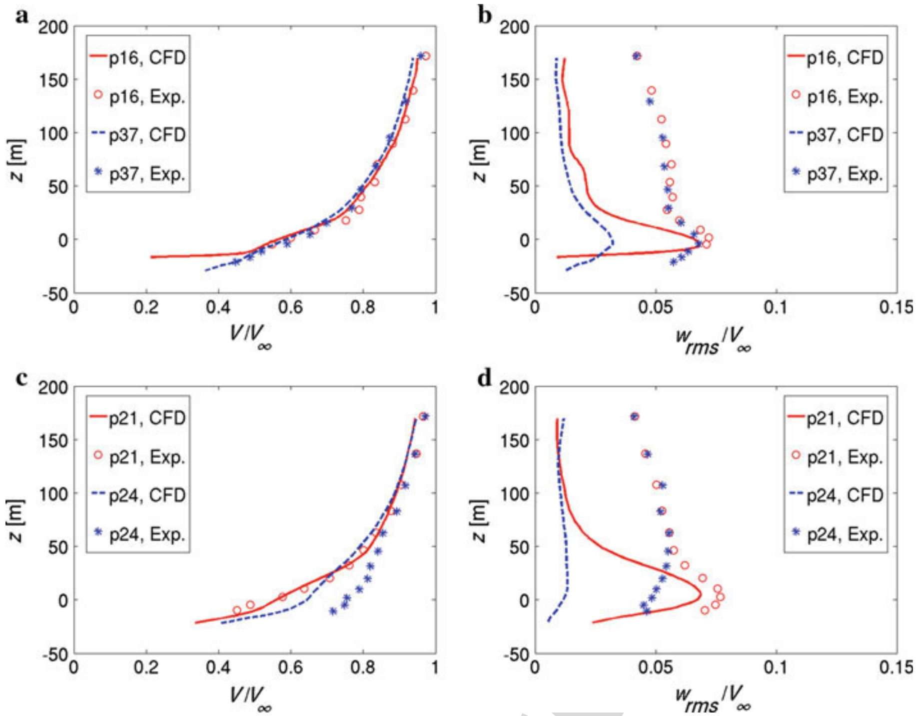

Fig. 3 Mean streamwise and root-mean-squared vertical velocities, scaled with mean inlet free-stream velocity. Vertical distance measured from the surface of pond 1, cf. Fig. 2

(cf. Fig. 2). The simulation results fit well with the experimental data, although the speed along `p24` is somewhat under-predicted. Considering its location in the terrain with very few upstream building structures, this discrepancy is likely to be due to errors in the inlet conditions.

The root-mean-squared (r.m.s.) values of vertical velocity are shown in Fig. 3b (locations `p03` and `p16`) and 3d (locations `p21` and `p24`). The general trends agree, and there is a consistency between the different locations, but the actual values from the simulation are generally much lower than those from the wind-tunnel experiment, particularly far from the ground ($z > 50$).

Interestingly, the r.m.s. levels of vertical velocity show a better agreement closer to the ground, i.e. in the more complex geometry, where the inlet conditions have less effect. This indicates that the turbulence levels in the simulation are considerably under-predicted due to errors in the boundary conditions rather than predicted dynamic evolution per se. This affects the solution throughout the domain, but to a much lesser degree at locations where turbulence is generated by geometry. For concentration predictions, the r.m.s. velocities at about the plume height (around $z = 0$ in the figures) are most significant. Here, the values agree well, at least in areas containing complex structures (such as `p16` and `p21`).

5.2 Contaminant Field

For illustrational purposes, a snapshot of the instantaneous concentration plume is shown in Fig. 4. Turbulent concentration fluctuations are evident in the figure.

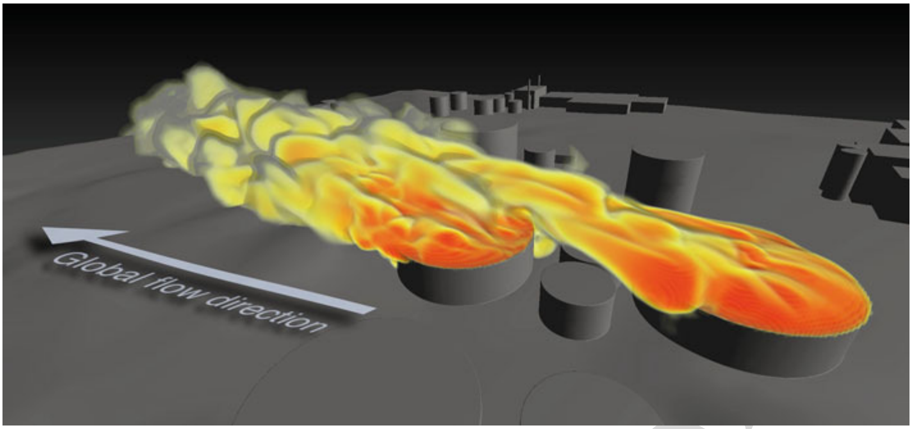

Fig. 4 A snapshot of the instantaneous concentration plume. *Red colour* high concentration; *yellow colour* low concentration. Created with VoluViz (Gaarder and Helgeland 2002)

Mean concentrations are shown in Fig. 5. Figure 5a shows the spanwise measuring lines `c03`, `c05` and `c07`, Fig. 5c shows the vertical measuring lines `c09`, `c11` and `c13`, and Fig. 5e shows the vertical measuring lines `c15`, `c16` and `c17`, cf. Fig. 2. The spanwise lines are always located 3 m above the ground. As can be seen, the simulation results agree well with the experimental data, especially `c05`, `c07`, `c11` and `c13`.

In Fig. 5a, the plume width is somewhat under-predicted in `c03`, but not significantly. Otherwise, the plume width is correctly computed. The ratios of simulated to measured plume width are 0.86 for `c03`, 0.90 for `c05` and 0.93 for `c07`, measured at a height corresponding to half of where the concentration peaks in each case, using linear interpolation of experimental data. The decay of the peak concentration fits well, but the location of the peak is somewhat misaligned.

The concentration along `c09` is over-predicted close to the ground, cf. Fig. 5c, possibly due to the plume misalignment discussed above. In contrast, the values higher up are somewhat under-predicted, which might be caused by the under-prediction of w_{rms}, cf. Fig. 3b.

The mean concentrations in Fig. 5e are consistent with the wind-tunnel measurements, but they are slightly under-predicted. Most likely this can be attributed to the slight misalignment of the concentration plume.

Figure 5b, d and f displays rms concentrations along the same vertical lines as the previous mean concentration plots. Figure 5b shows the spanwise measuring lines `c03`, `c05` and `c07`, Fig. 5d shows the vertical measuring lines `c09`, `c11` and `c13`, and Fig. 5f shows the vertical measuring lines `c15`, `c16` and `c17`. The predictions are consistent with each other, and the effect of the slight plume misalignment is apparent here as well. c_{rms}/C seems to be under-predicted somewhat throughout the domain compared to the experiments. On average, the CFD r.m.s. concentration is 42% of the mean for the listed locations, whereas in the experiments the r.m.s. concentration is 52% of the mean (both cases measured where the concentration is at its maximum). The difference between numerical and experimental r.m.s. to mean ratios is considered relatively minor.

Finally, Fig. 6 shows the decay of the peak concentration of the plume as it propagates through the domain. More specifically, the maximum values along several spanwise lines (including `c03`, `c05` and `c07`) are plotted versus their location in the streamwise direction.

Journal: **10546-BOUN** Article No.: **9711** MS Code: **BOUN901.3** ☐ TYPESET ☐ DISK ☐ LE ☐ CP Disp.:**2012/2/25** Pages: **20** Layout: **Small**

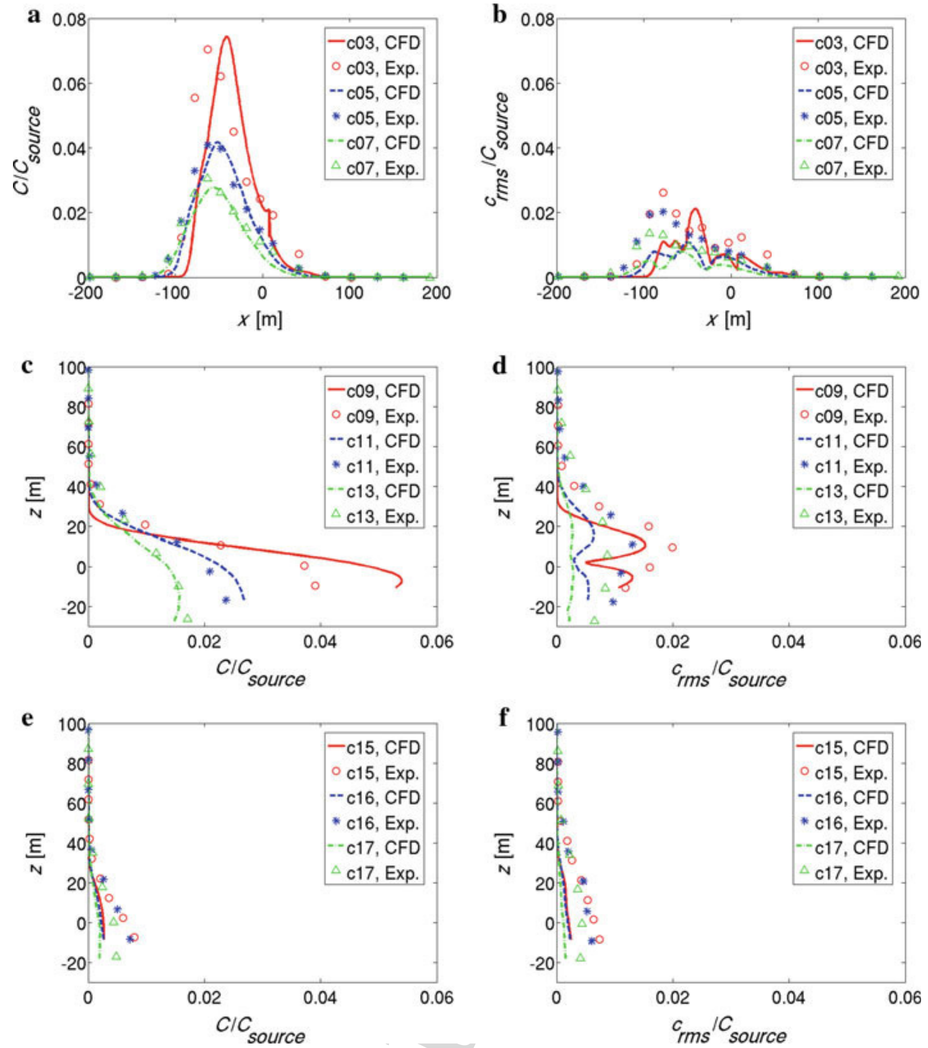

Fig. 5 Mean and root-mean-squared concentration values for various measuring lines, cf. Fig. 2. Distances (both *vertical* and *horizontal*) are measured from the surface centre of pond 1, also cf. Fig. 2

Note, (i) that this plot thus corrects for the plume misalignment, by following the plume maximum for both the experimental and computational case, and (ii) that the maximum value of C is sought out only in the spanwise direction, not vertically. As mentioned previously, the spanwise lines lie 3 m above the ground. The most interesting feature of the results in Fig. 6 is how well the decay is predicted in the computational model.

5.2.1 Statistical Analysis

In this section the overall performance of the simulations will be considered by using statistical performance measures to compare the simulated and experimental concentrations of the tracer gas, which was represented in the simulations by a passive scalar.

Journal: 10546-BOUN Article No.: 9711 MS Code: BOUN901.3 TYPESET DISK LE CP Disp.:2012/2/25 Pages: 20 Layout: Small

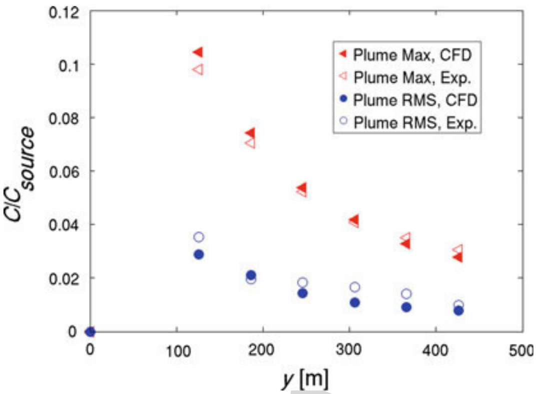

Fig. 6 Maximum values along several spanwise lines (including c03, c05 and c07, cf. Fig. 2) are plotted versus their location in the streamwise direction. Distance is measured from pond 1, cf. Fig. 2. The second, fourth and sixth locations along the *y*-axis correspond to the locations of the spanwise lines c03, c05 and c07

A large number of statistical performance measures have been proposed and used to evaluate dispersion models, see for example Chang and Hanna (2004). In the present case, the comparison will be performed using the metrics factor of two (*Fa2*), mean relative bias (*MRB*), fractional bias (*FB*), mean relative square error (*MRSE*), and normalized mean square error (*NMSE*), in line with the recommendations from the SMEDIS project (Carissimo et al. 2001) and the more recent COST 732 action (Schatzmann et al. 2010; Di Sabatino et al. 2011).

In the following discussion it is assumed that one has a set of predictions and observations, denoted by C'_p and C'_o, respectively. Measurement positions that lie close to the edge of the plume can make a disproportionally large impact on the computed values of the statistical performance measures. To overcome this, a threshold value is set, and the data are processed such that all values that are smaller than the threshold are set to the threshold value. Mathematically, one can write

$$C = \max(C', C_\mathrm{thresh}), \tag{8}$$

where C is the processed value that will be used in the comparison. In the present work the threshold $C_\mathrm{thresh} = 10^{-4}$ is employed. This is consistent with the sensitivity of the mean concentration measurements in the wind tunnel.

The results of dispersion models have traditionally been considered adequate if they give results within a *Fa2* of the reference data, i.e. if one has

$$C_\mathrm{o}/2 \leq C_\mathrm{p} \leq 2C_\mathrm{o}. \tag{9}$$

The *Fa2* performance measure is defined as the fraction of monitor locations where the following holds:

$$Fa2 = \frac{N|_{C_\mathrm{o}/2 \leq C_\mathrm{p} \leq 2C_\mathrm{o}}}{N_\mathrm{tot}}. \tag{10}$$

For the present simulation $Fa2 = 0.757$ is obtained, i.e. the predicted results are in the factor-of-two band for 76% of the measurement positions.

The *Fa2* metric only gives the fraction of the measurements that lie within the factor-of-two band. To obtain more information, other metrics must be considered. The *MRB* and *FB* are measures of over- or under-prediction defined by

$$MRB = \left\langle \frac{2(C_\mathrm{p} - C_\mathrm{o})}{C_\mathrm{p} + C_\mathrm{o}} \right\rangle, \tag{11}$$

$$FB = \frac{2\left\langle C_\mathrm{o} - C_\mathrm{p}\right\rangle}{\left\langle C_\mathrm{o} + C_\mathrm{p}\right\rangle}, \tag{12}$$

where the angular brackets denote an average over the entire dataset. Note the difference in sign of the two metrics, such that under-prediction is represented by a negative *MRB* value and a positive *FB* value and vice versa for over-prediction.

Related metrics are the *MRSE* and the *NMSE*. In additions to systematic errors, these metrics also quantify the variance of the difference between the compared datasets and is thus a measure of the scatter in the comparison of the predicted and observed values. The *MRSE* and *NMSE* are defined by

$$MRSE = 4\left\langle \left(\frac{C_\mathrm{p} - C_\mathrm{o}}{C_\mathrm{p} + C_\mathrm{o}}\right)^2 \right\rangle, \tag{13}$$

$$NMSE = \frac{\left\langle (C_\mathrm{o} - C_\mathrm{p})^2 \right\rangle}{\left\langle C_\mathrm{o}\right\rangle \left\langle C_\mathrm{p}\right\rangle}. \tag{14}$$

For the present simulation, $MRB = -0.284$, $FB = 0.032$ and $MRSE = 0.385$, $NMSE = 3.018$ are obtained. We note in passing that the computed *MRB* value corresponds to a systematic under-prediction of 25%, whereas over- and under-prediction almost cancel out for the *FB* metric.

When considered together, the *MRB*/*MRSE* and *FB*/*NMSE* pairs give information both on the level of over- and under-prediction and to what extent the predictions are consistent with the observations. This can be shown by noting that always,

$$MRSE \geq MRB^2, \tag{15}$$

$$NMSE \geq \frac{4FB^2}{4 - FB^2}. \tag{16}$$

with equality in the case of systematic over- or under-prediction. If *MRB* versus *MRSE* or *FB* versus *NMSE* is plotted, there will be an ‘ideal’ trend curve given by the lower bounds given above. The extent that a model result is consistent with the reference data can then be assessed by the distance to the trend curve.

The SMEDIS project (Carissimo et al. 2001) comprised a large number of cases and reference datasets. Of these, in particular, the cases EMUDJ and EMUNJ are of a comparable complexity to the present study. A scaled-down model of an industrial installation—located in Amlwch, Wales—and the surrounding countryside was constructed and wind-tunnel experiments were performed in the Surrey EnFlo facility during the Evaluation of Model Uncertainty (EMU) project (Cowan and Robbins 1996). The experimental data were later post-processed and scaled back to real scale by the SMEDIS project.

In Fig. 7 the computed *MRB* versus *MRSE* for the present calculation is shown. For comparison we also include results from a recent simulation of the EMUDJ case (Gjesdal et al. 2008) and average results from simulations performed by the SMEDIS project for the scenario categories *complex terrain* and *obstacles* (Carissimo et al. 2001). Note that the majority of *terrain* scenarios in SMEDIS were not from obstructed geometries. As a consequence, the performance measures for these cases may possibly be skewed away from the EMU scenarios.

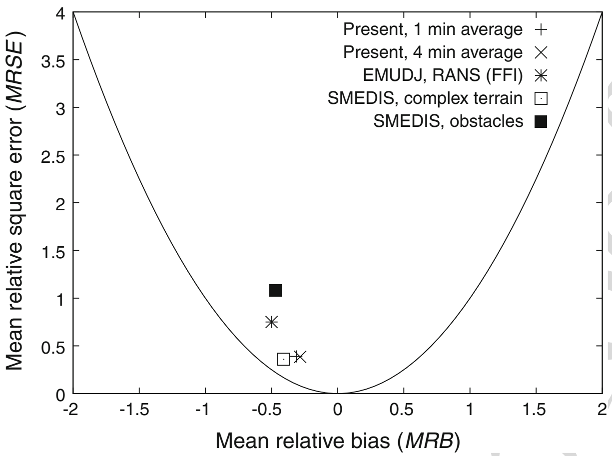

Fig. 7 Statistical performance measures, *MRB* versus *MRSE*, for the present simulation compared to an earlier simulation of the EMUDJ reference cases and SMEDIS results for scenarios characterized by complex terrain and obstacles, respectively

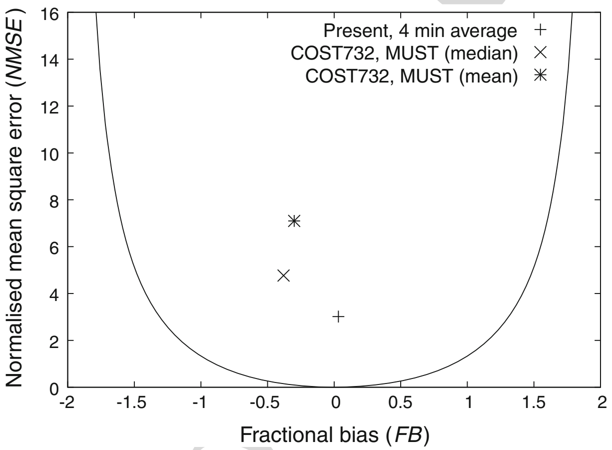

Fig. 8 Statistical performance measures, *FB* versus *NMSE*, for the present simulation compared to the corresponding median and mean quantities from the COST 732 comparison exercise of dispersion in the MUST obstacle array geometry

It is therefore probable that the performance measures for the EMU cases in SMEDIS lie somewhere between the two points.

Recently, the COST 732 Action (Schatzmann et al. 2010; Di Sabatino et al. 2011) performed a comparison of 18 different simulations of a dispersion scenario in the MUST obstacle array geometry. In Fig. 8 the computed *FB* and *NMSE* from the present simulations and the median and mean of the corresponding quantities from the COST 732 exercise are shown.

Journal: 10546-BOUN Article No.: 9711 MS Code: BOUN901.3 TYPESET DISK LE CP Disp.:2012/2/25 Pages: 20 Layout: Small

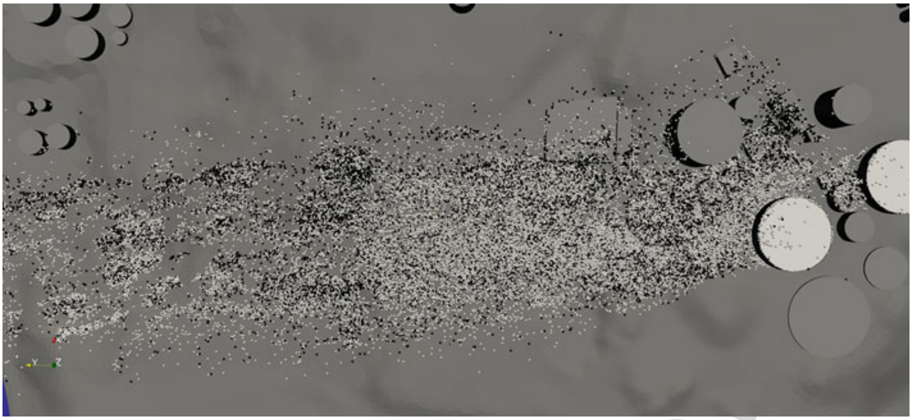

Fig. 9 Accumulated deposition at the end of the discrete particle simulation. *Dark colour* heavy particles; *light colour* light particles

5.3 Ground Deposition

Discrete particle transport was simulated primarily in order to predict particle deposition. More specifically, it is of interest to see if both the large (18 μm) and small (2 μm) particles are deposited at approximately the same rate, or if only the smaller aerosols are transported over longer distances. No experimental reference data are available for particle deposition, but in light of the previous results, it is likely that the simulation provides a good indication as to how particles emitted from the aeration ponds are deposited in the domain. Note that the following results are only tentative, as a more complete analysis requires knowledge of second-order effects (evaporation, agglomeration etc.), a much higher number of particles, and a longer release time, in order to approach statistical convergence.

Figure 9 shows the deposition on the ground and building roofs after all (>99%) released particles have left the domain or been deposited. Clearly, the deposition is chaotic, indicating the presence of turbulence. Within the near-field domain simulated here, there seems to be no significant difference in the deposition patterns for large and small particles. The simulation results show that 23% of the released particles are deposited, of which 58% are large particles. Hence, there is no significant differences between the deposition of large and small particles within the first few hundred metres downstream of the ponds.

6 Concluding Remarks

It has been demonstrated that computational fluid dynamics (CFD) can faithfully predict the aerial dispersion of aerosols at low Stokes numbers in complex industrial/urban terrain in the case of neutral conditions and flow in the high Reynolds number range. There is generally a good correspondence between the simulations and the experimental measurements, especially in the near-surface layer (0–50 m from the ground). In particular, the predicted decay of both the mean and r.m.s. concentrations are in excellent agreement with wind-tunnel experiments; the mean concentration 200 m downwind the plume is approximately 2% of the source strength 3 m from the ground. The r.m.s. concentration levels play an increasingly important role downwind as the mean concentration is reduced.

The results show that the plume emitted from the ponds remain narrow up to at least 500 m downwind (100–150 m wide), and that it grows very slowly in the vertical direction (40–50 m in height at 400 m downwind the ponds). Also, the maximum predicted/measured mean concentration remain very close to the ground ($\leq$3 m), whereas the concentration fluctuations attain their maxima 10–20 m above the ground. Vertical r.m.s. velocity fluctuations peak at around 10–30 m above the ground as well, close to where the r.m.s. concentration peaks. Finally, there seemed to be little difference in the deposition rates of large and small particles in the near-field. The results of this study also indicates that the rate at which aerosols emitted from the ponds are deposited constitutes a significant effect with respect to the expected overall concentration level further downwind.

In summary, CFD has proven to be a useful tool for analyzing, predicting and understanding aerosol dispersion in the neutral atmospheric boundary layer. The present study also demonstrates the large impact of the chosen inflow conditions in areas of the domain with little complex geometry (i.e. at high elevations). Further extensions of the methodology used herein, e.g. to stratified boundary layers will be investigated in a future study, in which stratified inflow will have to be generated in a separate periodic domain with ground heating or cooling.

Acknowledgments Part of this work was financially supported by Borregaard Ind. Ltd. and by the Norwegian Research Council through the Norwegian Center of Excellence Center for Biomedical Computing. We would like to thank Drs Anders Helgeland (FFI), Øyvind Andreassen (FFI), Janet M. Blatny (FFI), and Viggo Waagen (Borregaard Ind. Ltd.). The staff at the EnFlo laboratory at the University of Surrey, Guildford, UK, Prof Alan Robins and Dr Paul Hayden, are also acknowledged for their support during the project. Finally, the authors are grateful for valuable feedback from the reviewers.

References

Blatny JM, Reif BAP, Skogan G, Andreassen Ø, Høiby EA, Ask E, Waagen V, Aanonsen D, Aaberge IS, Caugant DA (2008) Tracking airborne *Legionella* and *Legionella pneumophila* at a biological treatment plant. Environ Sci Technol 42:7360–7367

Blatny JM, Fossum HE, Ho J, Tutkun M, Skogan G, Andreassen Ø, Fykse EM, Waagen V, Reif BAP (2011) Dispersion of legionella-containing aerosols from a biological treatment plant, Norway. Front Biosci 1(3):1300–1309

Carissimo B, Jagger SF, Daish NC, Halford A, Selmer-Olsen S, Riikonen K, Perroux J, Wurtz J, Bartzis J, Duim NJ, Ham K, Schatzmann M, Hall R (2001) The SMEDIS database and validation exercise. Int J Environ Pollut 16:614–629

Chang JC, Hanna SR (2004) Air quality model performance evaluation. Meteorol Atmos Phys 87(1–3): 167–196. doi:10.1007/s00703-003-0070-7

Coirier WJ, Fricker DM, Furmanczyk M, Kim S (2005) A Computational Fluid Dynamics approach for urban area transport and dispersion modeling. Environ Fluid Dyn 5:443–479

Cowan I, Robbins A (1996) Project EMU experimental data: case C1. Tech. Rep., EnFlo Research Centre, University of Surrey, pp 1–16

Di Sabatino S, Buccolieri R, Olesen HR, Ketzel M, Berkowicz R, Franke J, Schatzmann M, Schluenzen KH, Leitl B, Britter R, Borrego C, Costa AM, Castelli ST, Reisin TG, Hellsten A, Saloranta J, Moussiopoulos N, Barmpas F, Brzozowski K, Goricsan I, Balczo M, Bartzis JG, Efthimiou G, Starchenko AV (2011) COST 732 in practice: the MUST model evaluation exercise. Int J Environ Pollut 44(1–4, SI): 403–418. doi:10.1504/IJEP.2011.038442

Durbin PA, Reif BAP (2002) The elliptic relaxation method. In: Launder B, Sandham N (eds) Closure strategies for turbulent and transitional flows. Cambridge University Press, Cambridge pp 127–152

Elgobashi S (1994) On predicting particle-laden turbulent flows. Appl Sci Res 52:309–329

Fluent 6.3 User's Guide (2006) Fluent 6.3 User's Guide. Fluent, Inc., New Hampshire, USA

Franke J, Hellsten A, Heinke Schlünchen K, Carissimo B (2011) The cost 732 best practice guideline for CFD simulation of flows in the urban environment: a summary. Int J Environ Pollut 44(1/2/3/4):419–427

Gaarder T, Helgeland A (2002) VoluViz 1.0 Report. Tech. Rep. FFI/RAPPORT-2002/03449, FFI (Norwegian Defence Research Establishment), pp 1–25

Germano M, Piomelli U, Moin P, Cabot W (1991) A dynamic subgrid-scale eddy viscosity model. Phys Fluids A Fluid Dyn 3:1760

Gjesdal T, Bjerkelund JW, Bjerke A (2008) Simulation of chlorine release in an industrial facility—FLUENT and HPAC model results. FFI/RAPPORT 2008/01732, Forsvarets Forskningsinstitutt

Kaplan H, Dinar N (1996) A Lagrangian dispersion model for calculating concentration distribution within a built-up domain. Atmos Environ 30:4197–4207

Kim SE (2004) Large eddy simulation using unstructured meshes and dynamic subgrid-scale turbulence models. Technical Report AIAA-2004-2548. 34th Fluid Dynamics Conference and Exhibit, American Institute of Aeronautics and Astronautics, pp 1–7

Lee RL, Calhoun RJ, Chan ST, Leone J, Shinn JH, Stevens DE (2000) Urban dispersion CFD modeling, fact or fiction? In: 84th AMS meeting, third symposium on the urban environment, Davis, CA, USA

Lien FS, Yee E (2004) Numerical modelling of the turbulent flow developing within and over a 3D building array, part I: a high-resolution Reynolds-averaged Navier–Stokes approach. Boundary-Layer Meteorol 112:427–466

Lien FS, Yee E, Ji H, Keats A, Hsieh KJ (2006) Progress and challenges in the development of physically-based numerical models for prediction of flow and contaminant dispersion in the urban environment. Int J Comput Fluid Dyn 20:323–337

Morsi SA, Alexander AJ (1972) An investigation of particle trajectories in two-phase flow systems. J Fluid Mech 55(2):193–208

Nguyen TMND, Ilef S, Jarraud L, Rouil C, Campese D, Che S, Haeghebaert F, Ganiayre F, Marcel J, Etienne J, Desenclos JA (2006) A community-wide outbreak of Legionnaires disease linked to industrial cooling towers—how far can contaminated aerosols spread. J Infect Dis 193:102–111

Nygård K, Werner-Johansen Ø, Rønsen S, Caugant DA, Simonsen Ø, Kanestrøm A, Ask E, Ringstad J, Ødegård R, Jensen T (2008) An outbreak of Legionnaires disease caused by long-distance spread from an air scrubber in Sarpsborg. Clin Infect Dis 46:61–69

Olsen JS, Aarskaug T, Thrane I, Pourcel C, Ask E, Johansen G, Waagen V, Blatny JM (2010) Alternative routes for dissemination of legionella pneumophila causing three outbreaks in norway. Environ Sci Technol 44:8712–8717

Robins A, Castro I, Hayden P, Steggel N, Contini D, Heist D (2001) A wind tunnel study of dense gas dispersion in a neutral boundary layer over a rough surface. Atmos Environ 35:2252–4243

Santiago JL, Martilli A, Martin F (2007) CFD simulation of airflow over a regular array of cubes Part I: Three-dimensional simulation of the flow and validation with wind-tunnel experiments. Boundary-Layer Meteorol 122:609–634

Schatzmann M, Olesen H, Franke J (eds) (2010) COST 732 Model evaluation case studies: approach and results. University of Hamburg, ISBN 3-00-018312-4

Sykes RI, Gabruk RS (1996) A second-order closure model for the effect of averaging time on turbulent plume dispersion. J Appl Meteorol 36:1033–1045

Taylor PA, Salmon JR (1993) A model for the correction of surface wind data for sheltering by upwind obstacles. J Appl Meteorol 49:226–239

Wang BC, Yee E, Lien FS (2008) Experimental and numerical study of contaminant dispersion in an array of cubic obstacles. In: Proceedings of the 7th international symposium on engineering turbulence modelling and measurements (ETMM7), pp 64–69

Journal: **10546-BOUN** Article No.: **9711** MS Code: **BOUN901.3** ☐ TYPESET ☐ DISK ☐ LE ☐ CP Disp.:**2012/2/25** Pages: **20** Layout: **Small**